JOURNAL OF GEOPHYSICAL RESEARCH, VOL. 115, B03411, doi:10.1029/2009JB006603, 2010

Timing and magnitude of shortening within the inner fore arc of the Japan Trench

Christine Regalla,[1] Donald Fisher,[1] and Eric Kirby[1]

Received 10 May 2009; revised 15 September 2009; accepted 19 October 2009; published 17 March 2010.

[1] New structural data and kinematic modeling provide evidence for Plio-Quaternary, inner fore-arc shortening inboard of the Japan Trench, northeastern Honshu, accommodated by the Futaba fault, a high-angle, basement-involved fault that bounds the Abukuma massif on the east. Significant throw along the Futaba fault associated with exhumation of the massif is implied by a regionally extensive footwall syncline, the absence of Neogene sediments in the hanging wall, and high relief in the hanging wall adjacent to the fault. Kinematic fault-related fold modeling best reproduces fold geometry with 2.0–3.1 km of dip slip along a 40°–55° west dipping reverse fault. At the southern tip of the fault, tephra horizons of known age within units that predate and postdate deformation bracket the onset of deformation to 3.95–5.6 Ma and are used to calculate an average slip rate of 0.5–0.7 mm/yr, a throw rate of 0.3–0.5 mm/yr, and a shortening rate of 0.3–0.5 mm/yr. The northeastern Japan subduction zone is viewed as a classic example of an erosive margin, where offshore subsidence records have been used to argue for Neogene basal erosion of the upper plate. Tectonic erosion rates have been estimated from reconstructions of the paleomargin that assume no upper plate deformation and temporally constant fore-arc taper. Evidence presented here for Neogene fore-arc shortening, however, suggests that the upper plate is deformable and implies that that offshore subsidence records may reflect a combination of tectonic erosion and upper plate shortening.

Citation: Regalla, C., D. Fisher, and E. Kirby (2010), Timing and magnitude of shortening within the inner fore arc of the Japan Trench, *J. Geophys. Res.*, *115*, B03411, doi:10.1029/2009JB006603.

1. Introduction

[2] Nearly half of the Earth's subduction boundaries are characterized as erosive margins that are interpreted to experience a net removal of upper plate material by upward migration of the plate boundary [*Scholl et al.*, 1980; *von Huene and Scholl*, 1991; *Clift and Vannucchi*, 2004]. Evidence for basal tectonic erosion comes primarily from offshore subsidence records argued to reflect thinning of fore-arc crust with little to no internal deformation of the upper plate [*Scholl et al.*, 1980; *von Huene and Lallemand*, 1990; *von Huene and Scholl*, 1991; *Lallemand et al.*, 1992]. Outer fore-arc subsidence records have been used to estimate average rates of tectonic erosion comparable to globally averaged rates of accretion [e.g., *von Huene and Lallemand*, 1990; *Lallemand et al.*, 1992], suggesting that erosive margins play an integral role in global crustal cycling. The convergent plate boundary inboard of the Japan Trench (Figure 1) is considered a type example of an erosive margin [e.g., *Scholl et al.*, 1980; *von Huene and Lallemand*, 1990; *von Huene and Scholl*, 1991; *Clift and Vannucchi*, 2004]. Neogene tectonic erosion in northeastern Japan has been inferred from offshore subsidence documented by benthic foraminifera assemblages recovered from Deep Sea Drilling Project (DSDP) sediment cores and multichannel seismic reflection profiles that image a basal Miocene unconformity 5–6 km below sea level [*von Huene et al.*, 1978; *Arthur et al.*, 1980; *Keller*, 1980; *Nasu et al.*, 1980; *von Huene and Culotta*, 1989; *von Huene and Lallemand*, 1990; *von Huene et al.*, 1994; *Niitsuma*, 2004]. Nearly all estimates of tectonic erosion rates for northeastern Japan are based on reconstructions of the paleomargin that assume a temporally constant fore-arc taper with no upper plate deformation [e.g., *von Huene and Lallemand*, 1990; *Lallemand et al.*, 1992]. This study presents evidence, however, for Neogene shortening across the upper plate inboard of the Japan Trench, accommodated by the Futaba fault. This observation suggests that subsidence occurs outboard of a deformable fore arc and that outer fore-arc evolution may reflect a combination of processes related to both basal erosion and upper plate deformation.

[3] Late Neogene shortening throughout the island of Honshu is well documented along a network of reverse faults and fault-related folds across the northeastern Japan arc that record contractional deformation, basin inversion,

[1]Department of Geosciences, Pennsylvania State University, University Park, Pennsylvania, USA.

0148-0227/10/2009JB006603

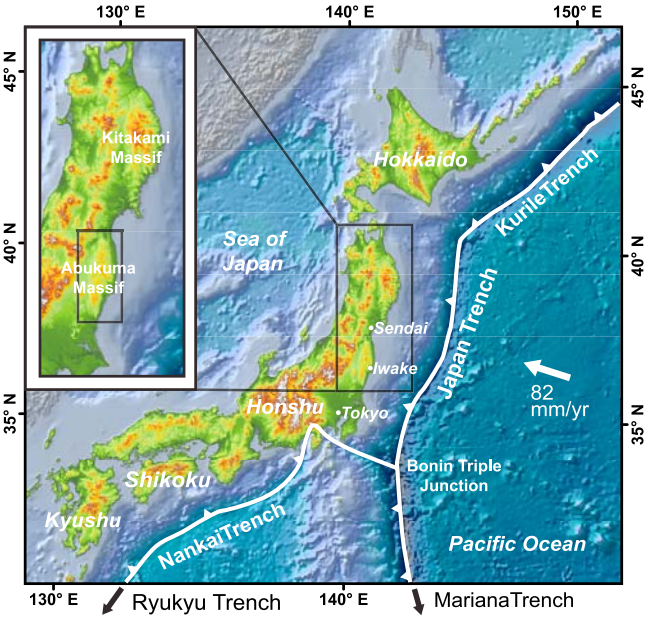

Figure 1. Digital elevation model and bathymetry of Japan showing tectonic boundaries and the locations of the basement-cored Abukuma and Kitakami massifs. The Japan Trench marks the eastern boundary of the North American plate, where the Pacific plate subducts nearly orthogonal to the margin at a rate of 82 mm/yr. Elevation and bathymetry were obtained from SRTM3 and ETOPO2 data sets.

and differential uplift of rock [e.g., *Sato and Amano*, 1991; *van der Werff*, 2000; *Sato et al.*, 2002; *National Institute of Advanced Industrial Science and Technology* (*AIST*), 2008]. Several east vergent contractional structures in the arc and western fore arc are interpreted to reflect Plio-Quaternary inversion of Miocene rift-related basins [*Sato et al.*, 2002; *Kato et al.*, 2006]. Recent earthquakes along faults at the eastern edge of the volcanic arc are consistent with east vergent reverse slip [e.g., *Hikima and Oki*, 2008]. Although fore-arc shortening has not previously been documented, significant shortening is suggested by the presence of topographically high, deeply incised basement massifs along the margin (Abukuma and Kitikami massifs, Figure 1) that have uplifted marine terraces along their eastern flanks [*Suzuki*, 1989; *Kioke and Machida*, 2001; *Kubo et al.*, 2002].

[4] The southernmost basement massif, the Abukuma massif, is bound on the east by the regionally extensive Futaba fault system (Figures 1 and 2). Previous workers have interpreted the Futaba fault as a vertical to near-vertical fault with predominantly left-lateral Quaternary slip, based

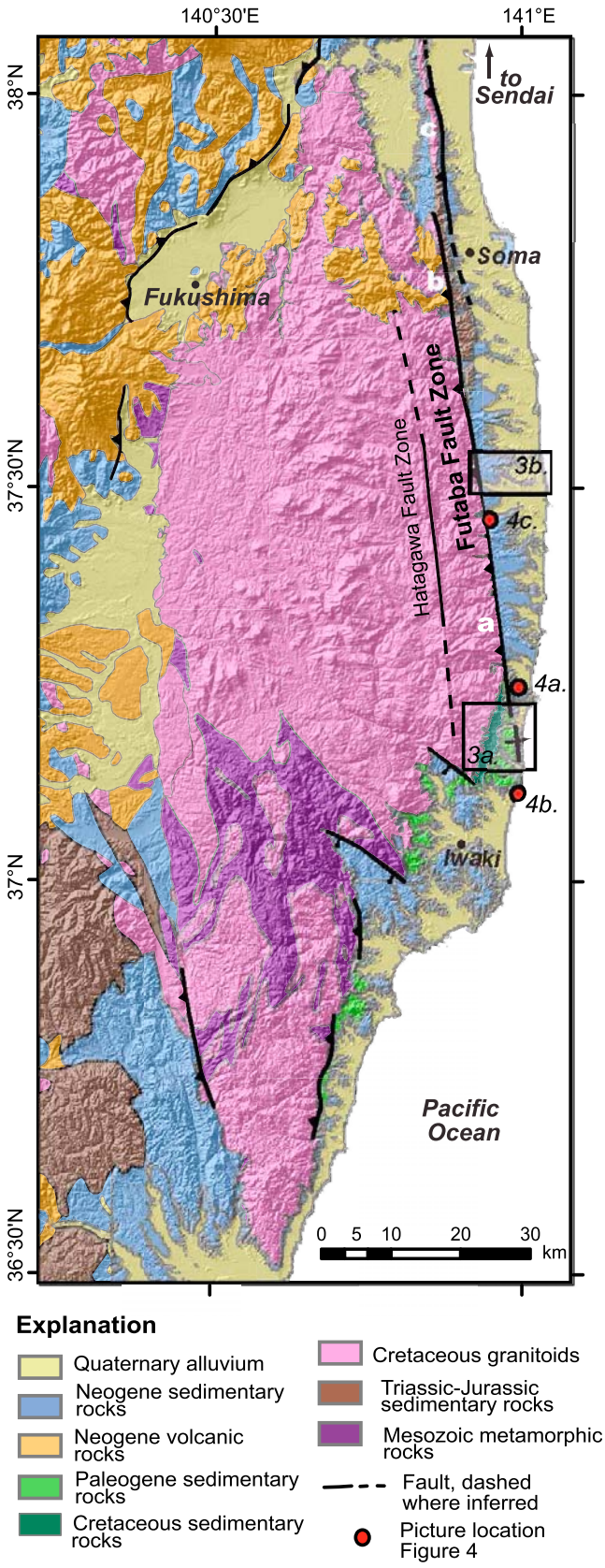

Figure 2. Simplified geologic map of the Abukuma massif [after *Chishitsu*, 2003; *Kubo et al.*, 2003] showing locations of active faults [after *AIST*, 2008]. The Futaba fault is divided into the a, Namie segment; b, Haramachi segment; and c, Watari segment. Cretaceous granites and Mesozoic sedimentary and metamorphic rocks core the massif, and stream cuts expose deformed Paleogene and Neogene strata in the footwall of the Futaba fault. Boxes denote locations of inset geologic maps in Figure 3.

on trenching of the central segment and collocation with a Cretaceous sinistral shear zone [*Fukushimaken*, 1998, 1999; *Tomita et al.*, 2002; *Kubo et al.*, 2003; *Ohtani et al.*, 2004; *AIST*, 2008]. However, new field observations presented here suggest that the Futaba fault is a steep, west dipping fault with a sizable dip slip component, that places Cretaceous granites in fault contact with a Neogene cover sequence and generates a fault-related fold for ~150 km along strike. In this study, structural data from the southern Futaba fault are used as inputs in a kinematic fault-related fold model to constrain subsurface fault geometry and total dip slip. These results are combined with biostratigraphic ages and tephrachronology in units that bracket the onset of fault-related folding to estimate the timing and rates of deformation, and provide evidence for significant late Neogene shortening in the inner fore arc inboard of the Japan Trench.

2. Geologic Background

2.1. Tectonic History

[5] The Abukuma massif is a basement-cored highland within the inner fore arc of northeastern Honshu, inboard of the Japan Trench (Figure 1). The Japan Trench marks the eastern boundary of the North American plate, where the Pacific plate subducts near-orthogonal to the plate margin at a rate of 82 mm/yr [*Seno et al.*, 1993; *Niitsuma*, 2004]. Subduction along the western Pacific margin initiated during the middle Mesozoic and Cretaceous arc volcanism led to the emplacement of voluminous granodioritic plutons beneath the arc [*Hiroi et al.*, 1998; *Iwata et al.*, 2000]. Cretaceous granites have been imaged within the basement beneath the fore-arc slope cover sequence up to 150 km east of the present-day arc [*Finn*, 1994]. Early to middle Miocene (25–15 Ma) back-arc extension led to the rifting of the eastern Asian margin, the opening of the Sea of Japan, and the formation of the modern Japan arc [*Sato and Amano*, 1991; *Jolivet et al.*, 1994; *Sato*, 1994]. Relict Miocene rift-related half grabens extend across western Honshu and have been recognized as far to the east as the arcward margin of the Abukuma and Kitakami massifs [*Sato and Amano*, 1991; *Sato et al.*, 2002; *Kato et al.*, 2006].

[6] Subsidence of the outer fore arc of the northeastern Japan margin initiated in the early Miocene and has continued through the Pliocene to present [*von Huene and Lallemand*, 1990]. Offshore subsidence is documented in multichannel seismic profiles that image a basal Neogene unconformity 5–6 km below sea level and 15–30 km from the trench [*von Huene and Culotta*, 1989; *von Huene et al.*, 1994; *Niitsuma*, 2004] and benthic foraminifera assemblages recovered from DSDP sediment cores that record a progressive deepening of the upper slope since 22 Ma [*von Huene et al.*, 1978; *Arthur et al.*, 1980; *Keller*, 1980; *Nasu et al.*, 1980; *von Huene and Lallemand*, 1990]. These data have been used to estimate average trench retreat rates of ~3 km/Ma and the subsequent removal of 55 km^2/Ma of material from the upper plate since the early Miocene [*von Huene and Lallemand*, 1990; *Lallemand et al.*, 1992; *von Huene et al.*, 1994; *Niitsuma*, 2004].

[7] The northeastern Japan arc transitioned into a contractional regime during the late Miocene to early Pliocene [*Sato*, 1994]. The initiation of reverse motion is bracketed to 4.3–2.4 Ma in the back arc along the Japan Sea coast [*Awata*, 1988; *Sato*, 1994], but the cause and initiation of compression across the arc are not well constrained [e.g., *Sato and Amano*, 1991; *Sato*, 1994]. Neogene shortening has been documented across a network of contractional structures extending from the Sea of Japan to the arcward flanks of the Abukuma and Kitakami massifs [*Sato*, 1994; *van der Werff*, 2000], and many of these fault systems remain active today [*Wesnousky et al.*, 1984; *AIST*, 2008; *Hikima and Oki*, 2008]. Several of these contractional structures have been identified as high-angle, basement-involved faults interpreted to reflect positive basin inversion of preexisting Miocene extensional grabens [*Sato et al.*, 2002; *Kato et al.*, 2006], implying that modern day shortening may occur along reactivated Miocene extensional faults. The Futaba fault is the most trenchward, onshore fault east of this system of Neogene contractional structures. The fault is ~150 km in strike length and places Cretaceous granites of the Abukuma massif in fault contact with Neogene sedimentary rocks.

2.2. Stratigraphy

[8] The basement of northeastern Honshu consists of Cretaceous plutonic rocks, remnant Paleozoic margin rocks, and a middle Mesozoic subduction complex that were rifted from the Asian mainland during Miocene back-arc extension. Basement units are exposed in the hanging wall of the Futaba fault, in the Abukuma massif (Figure 2), and are unconformably overlain by an upper Cretaceous through Quaternary sequence of marine and terrestrial siliciclastics and volcanic rocks [*Mitsui*, 1971; *Machida*, 1999; *Kubo et al.*, 2003; *Suto et al.*, 2005].

[9] The upper Cretaceous Futaba Group, Paleogene Shiramizu Group, and Miocene Yunagaya, Shirado, Takuku, and Taga groups (Figure 3) consist of marine and terrestrial sequences of conglomerate, sandstone, mudstone, and siltstone with intercalated coal seams and tephras [*Mitsui*, 1971]. Cretaceous units are only exposed at the southern tip of the Futaba fault, and the total thickness of upper Cretaceous to Oligocene units ranges from 950 to 1100 m. Miocene units are exposed in the footwall of the Futaba fault along its entire strike length [*Kubo et al.*, 2003]; the total thickness of the Miocene section ranges from 800 to 2200 m [*Kubo et al.*, 2002; *Suto et al.*, 2005]. The entire sedimentary cover sequence in the footwall of the Futaba fault thins northward from the southern fault tip [*Kubo et al.*, 2002; *Suto et al.*, 2005].

[10] The Sendai Group consists of nearshore sandstones and mudstones that lie unconformably atop Miocene units [*Suto et al.*, 2005, Figure 3]. The Mukaiyama and Dainenji formations of the upper Sendai Group are deformed in the footwall along the central portion of the Futaba fault, but the lower Dainenji Formation onlaps the fault-related fold at the southern tip of the Futaba fault (Figure 3a). Numerous tephras are interbedded in the Sendai Group, and marker horizons are identified east of the Abukuma massif in the Dainenji and Mukaiyama formations [*Machida*, 1999; *Kubo et al.*, 2002]. A Pliocene tephra stratigraphy has been developed and correlated to an established biostratigraphic framework for the Neogene sediments [*Machida*, 1999; *Kubo et al.*, 2002; *Suto et al.*, 2005], and provides age constraints for the timing of Neogene deformation. The total

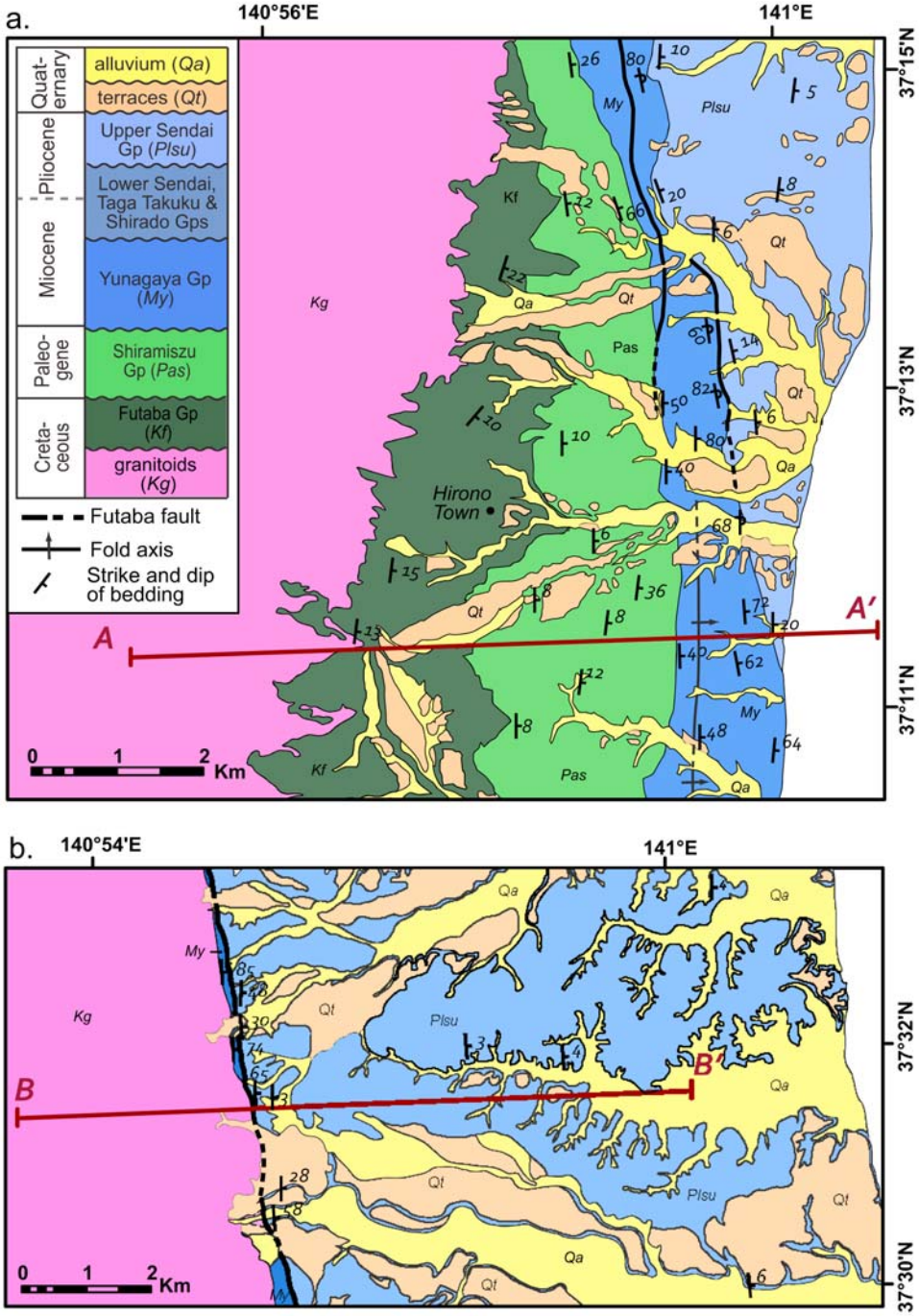

Figure 3. Geologic maps at locations of modeled transects across the (a) hanging wall anticline and (b) the footwall syncline, using the stratigraphy for the eastern flank of the Abukuma massif of *Suto et al.* [2005]. See Figure 2 for locations.

exposed thickness of the Sendai Group is ~300 m [*Kubo et al.*, 2002].

2.3. Futaba Fault

[11] The Futaba fault system extends for ~150 km along the eastern margin of the Abukuma massif, from northeast of Iwaki to southwest of Sendai (Figure 2). The fault zone parallels a Cretaceous, midcrustal, mylonitic, sinistral shear zone, which is overprinted by Neogene gouge and breccia [*Tomita et al.*, 2002; *Ohtani et al.*, 2004]. A Paleogene to early Neogene history of extensional faulting near the southern tip of the Futaba fault is inferred from segmentation of the sedimentary section into minor fault-bound subbasins. Neogene dip displacement of less than 200 m has been interpreted to reflect reactivation of these earlier structures [*Mitsui*, 1971].

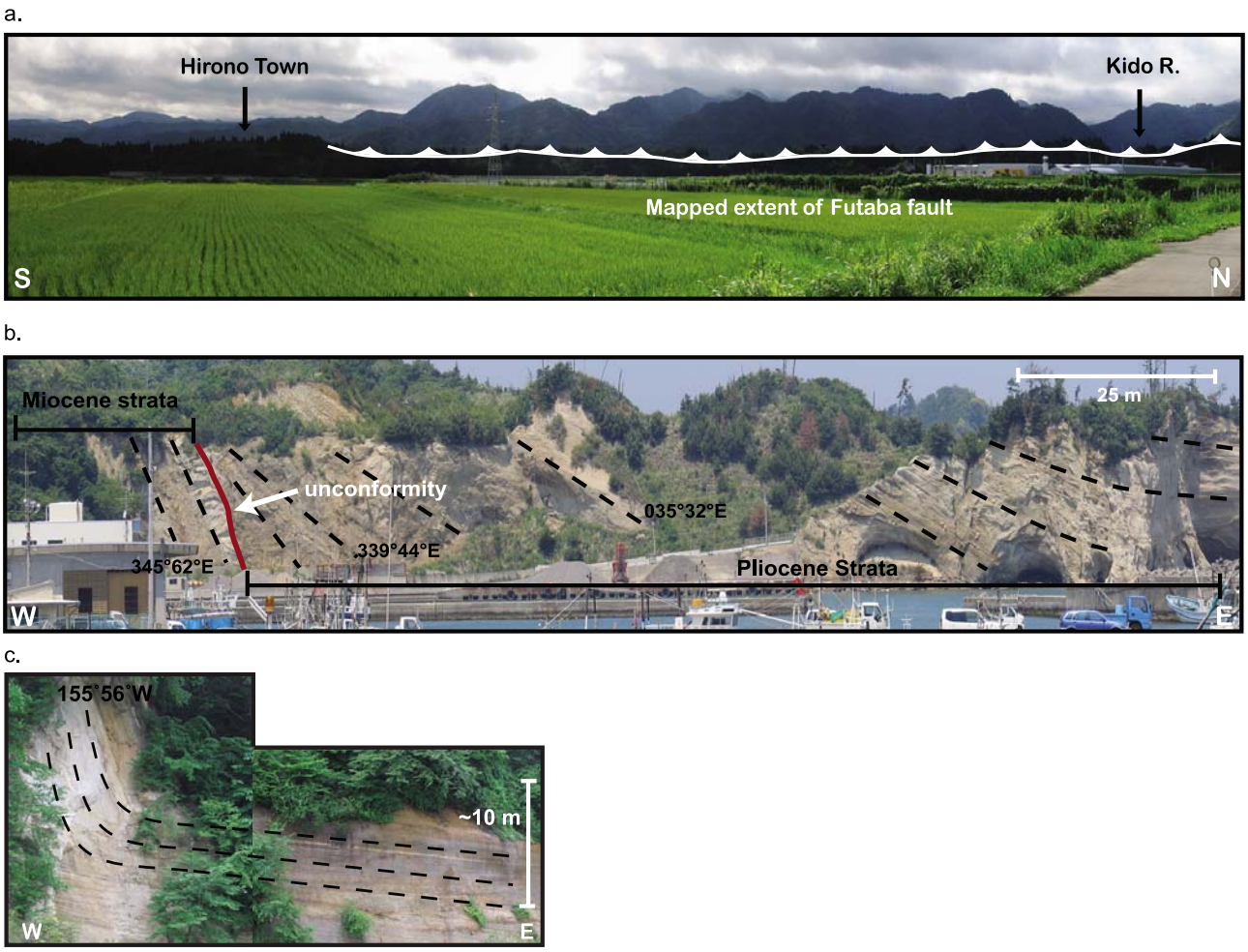

Figure 4. (a) Panorama of the Abukuma mountain front at the southern tip of the Futaba fault. Note the increase in maximum hanging wall elevation and relief where the Futaba fault becomes emergent. (b) An unconformity at the southern tip of the Futaba fault separates Miocene predeformational units of the Yunagaya Group from the Pliocene strata of the Dainenji Formation, upper Sendai Group, deposited after the onset of deformation. (c) Footwall syncline developed in the Dainenji Formation along the Namie segment of the Futaba fault. See Figure 2 for locations.

[12] Previous tectonic studies have reported dips for the Futaba fault that range from 90°–35° to the west [*Mitsui*, 1971; *Fukushimaken*, 1999] and have argued for both left-lateral and minor reverse displacement [*Mitsui*, 1971; *Fukushimaken*, 1999; *Kubo et al.*, 2003]. Fault characterizations by the Active Faults Research Center of Japan classify the modern Futaba fault as a subvertical (80°W–90°) fault with dominantly left-lateral displacement [*Fukushimaken*, 1998, 1999; *Kubo et al.*, 2003]; however, the fault is not cataloged among an inventory of active thrust faults in Japan [i.e., *Ikeda et al.*, 2002]. The Futaba fault is divided into the southern Namie segment, the central Haramachi segment, and the northern Watari segment (labels a–c in Figure 2). Quaternary ruptures are recognized along only the Haramachi segment, where Quaternary alluvium is offset, producing a 1.2 m high east facing scarp [*Fukushimaken*, 1998, 1999; *Kubo et al.*, 2003]. Ruptures at 2400 and 10,000 years B.P. are reported from a trench across the fault near Soma, and offset deposits yield a left lateral slip rate of 0.05–0.15 mm/yr and a dip slip rate of 0.05–0.1 mm/yr [*Fukushimaken*, 1998, 1999]. The Watari and Namie segments are not categorized as active, as offset Quaternary deposits have not been observed along these segments [i.e., *AIST*, 2008]; however, their continuity with the active Haramachi segment and the presence of a deeply incised, steep, linear mountain front along the entire fault suggests the potential for Quaternary activity (Figure 4a).

3. Neogene Deformation Associated With the Futaba Fault

[13] New field observations and interpretation of existing geologic maps provide evidence that the Futaba fault is a steep, west dipping reverse fault that has been active since the late Neogene. Reverse slip along a steep, west dipping fault is supported by an east vergent fault-related fold, west dipping reverse shear planes in the fault zone, and the absence of the sedimentary cover sequence in the hanging

wall. The Futaba fault places crystalline basement in fault contact with folded Cretaceous through Pliocene sedimentary rocks along ~150 km of strike length. The cover sequence is preserved in the hanging wall of the Futaba fault only at the southern tip of the Namie segment, where the Futaba fault is blind and the Cretaceous through Miocene section is folded into an open, gently southward plunging, hanging wall anticline (Figure 3a). Bedding dips increase from ~5°E in the gently dipping western limb of the of the hanging wall anticline to subvertical or overturned in the steeply dipping eastern limb, with bedding dips that range from ~60°E to 60°W. The deposition of these units predate deformation of the fault-related fold.

[14] Steeply dipping Miocene rocks in the forelimb of the anticline at the southern tip of the fault are unconformably overlain by gently dipping Pliocene strata of the Dianenji Formation (Figure 4b). Bedding dips in the Pliocene section at the southern tip of the fault decrease to the east from ~60°E directly above the unconformity to subhorizontal over a distance of ~150 m (Figure 4b). The unconformity at the southern tip of the Futaba fault transitions northward into a conformable contact with the underlying Mukaiyama Formation [*Kubo et al.*, 2002; *Kubo et al.*, 2003], and is interpreted here as a progressive unconformity separating units that predate the onset of deformation from units deposited during the growth of the fault-related fold. The timing of initiation of slip along the Futaba fault is therefore bracketed by the ages of units directly above and below the unconformity. Multiple tephra horizons interbedded in Miocene and Pliocene section have been correlated to a regional tephra stratigraphy [*Yoshida*, 1998; *Machida*, 1999] and provide age constraints to bracket the onset and rates of deformation.

[15] The hanging wall anticline at the southern tip of the Futaba fault is disrupted by minor reverse faults with displacements averaging less than 50 m [*Mitsui*, 1971; *Kubo et al.*, 2003]. An eastern splay of the Futaba fault has a dip of 50°W and places overturned beds of the Miocene Yunagaya Group in the forelimb of the hanging wall anticline on top of gently east dipping beds of the Pliocene Dainenji Formation (Figure 3a). Other measured minor faults in the region have dips ranging from 35° to 85°.

[16] The Pliocene units above the unconformity at the southern tip of the Futaba fault are folded into a regionally extensive footwall syncline that extends along the northern ~40 km of the Namie segment. The Dainenji and Mukaiiyama formations of the upper Sendai Group are exposed along two stream cuts across the footwall syncline (Figure 4c). The fault contact between Cretaceous basement and the sedimentary cover sequence is not exposed in outcrop, but Riedel shears exposed in a quarry in the fault zone are consistent with slip along a steep, west dipping reverse fault. The most common shear plane orientation has a west dip of 50°–60° and offset markers indicate top to the east displacement.

[17] Ongoing exhumation of the Abukuma massif associated with slip along the Futaba fault is supported by mountain front morphology and patterns of incision within the massif. The northward transition of the Futaba fault from blind to emergent at its southern tip is expressed in the landscape by the emergence of a steep, linear mountain front, an increase in the average elevation of the massif, and an increase in hanging wall relief (Figure 4a). Additionally, high hillslope gradients and deeply incised channels in the massif are restricted to an ~10–15 km region adjacent to the Futaba fault and hanging wall channels contain prominent knickzones, suggesting recent adjustments in channel and hillslope gradient in response to topographic gradients associated with slip along the fault.

4. Reconstructing Displacement Along the Futaba Fault

[18] The Futaba fault and the Abukuma massif northeastern Honshu, Japan, exhibit several characteristics in common with Laramide-style structures in the western United States [e.g., *Erslev*, 1991]. These include (1) involvement of crystalline basement in the hanging wall of the thrust, (2) a relatively sharp fault that places crystalline basement in contact with the sedimentary cover sequence, and (3) a diffuse zone of deformation and folding within the cover sequence. The trishear kinematic model replicates these characteristics of basement-involved deformation as the result of distributed simple shear within a triangular shear zone that propagates with the fault tip [*Erslev*, 1991]. This kinematic model has been used as an alternative to kink band fold kinematics to explain the downward tightening and convergence of fold hinges and changes in stratigraphic thickness and limb dip observed in basement-involved, fault-related folds [*Erslev*, 1991; *Allmendinger*, 1998]. Deformation produced by the trishear kinematic model is well matched by mechanical models that simulate basement-involved folds based on viscous folding theory for a homogenous, isotropic body [*Johnson and Fletcher*, 1994; *Johnson and Johnson*, 2002; *Cardozo et al.*, 2003]. Mechanical and kinematic models for basement structures have been shown to produce comparable deformation patterns within homogeneous, weak materials [*Hardy and Finch*, 2006], such as the poorly consolidated sediments that constitute the cover sequence of the Abukuma massif.

4.1. Trishear Kinematic Model

[19] Fault ramp angle and displacement required to produce the fold along the southern Futaba fault are constrained using a kinematic model implemented in MATLAB based on the forward modeling approach and velocity field of *Allmendinger* [1998] and *Zehnder and Allmendinger* [2000]. The trishear kinematic model produces simple shear within a triangular zone ahead of a propagating fault tip in a domain bound by a fixed footwall ($v = 0$) and a hanging wall with constant velocity, ($v = v_o$) over a given time step [*Erslev*, 1991; *Allmendinger*, 1998]. This model solves for a velocity field that describes the 2-D deformation of an incompressible material confined to a shear zone of angular area $\phi_1 + \phi_2$, whose apex is fixed to the propagating fault tip (Figure 5a). Material within the shear zone is deformed such that the divergence of the velocity field is zero, and produces area-balanced cross sections.

[20] The velocity field solution used here assumes homogenous trishear, such that $\phi_1 = \phi_2 = \phi$, for a v_x field that is linear in y [after *Zehnder and Allmendinger*, 2000]. At time $t = t_i$, the 2-D velocity field within the shear zone that

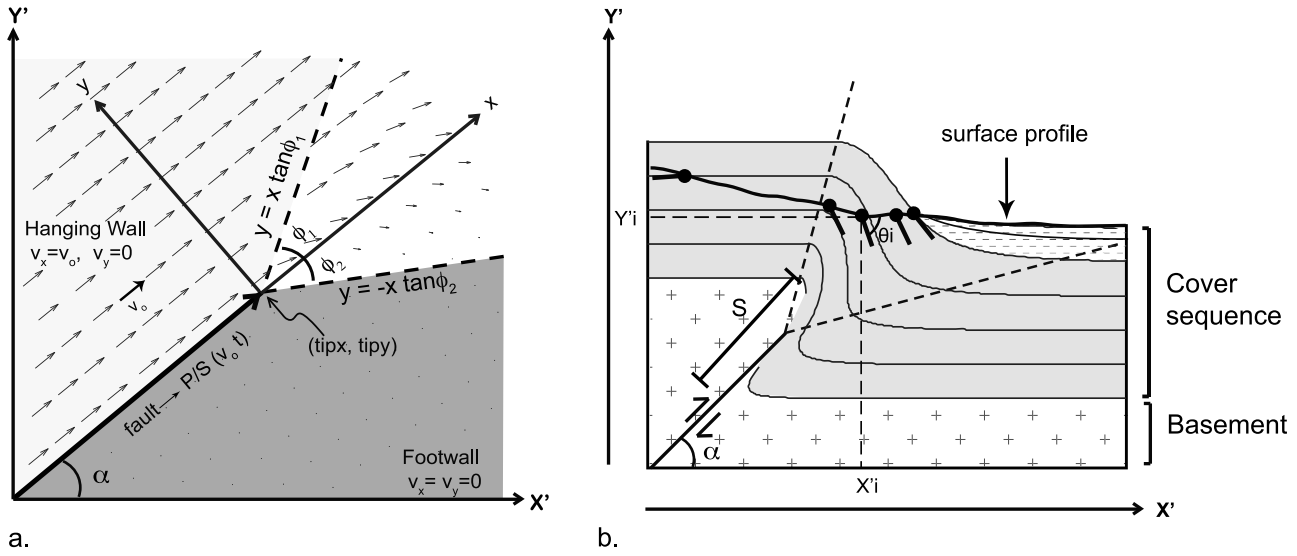

Figure 5. (a) Velocity field for the trishear kinematic model used to constrain Futaba fault geometry (model after *Zehnder and Allmendinger* [2000]). A fault-related fold is generated by distributed simple shear within a triangular zone of width $\phi_1 + \phi_2 = \phi$, bound by $y = x \tan \phi_1$ and $y = -x \tan \phi_2$, fixed to a propagating fault tip (tip_x, tip_y) in a tip-centered, x, y coordinate system. Deformation of bedding is simulated by numeric integration of the velocity field in an X′, Y′ coordinate system as the shear zone propagates with the fault tip. (b) Schematic showing a simulated fold geometry and bedding dip data (x_i, y_i, θ) along a surface profile. Quality of fit is assessed from the RMS misfit between observed bed dips and model bed slopes. Fault ramp angle (α) and total slip (S) are estimated from best fit parameter values.

satisfies the above assumptions and boundary conditions is prescribed by

$$v_x = \frac{v_o}{2}\left[\operatorname{sgn}(y)\left(\frac{|y|}{x\tan\varphi}\right)^{1/s} + 1\right]$$
$$v_y = \frac{v_o \tan\varphi}{2(1+s)}\left[\left(\frac{|y|}{x\tan\varphi}\right)^{(1+s)/s} - 1\right] \quad (1)$$

where $s = 1$ [*Zehnder and Allmendinger*, 2000]. This velocity field solution is similar to those generated in mechanical models of trishear-like deformation within an incompressible, elastic-plastic material [*Cardozo et al.*, 2003].

4.2. Simulation of Deformation

[21] The shape of a fault propagation fold in a trishear model is controlled by the geometry of the shear zone and the rate and direction in which it propagates through the deforming media. This is dictated by six model parameters: (1) ϕ, the angular width of the shear zone, or the trishear angle, (2) α, the fault ramp angle, (3) (tip_x, tip_y), the x and y coordinates describing the position of the fault tip, (4) v_o, slip rate, or hanging wall velocity, (5) P/S ratio, the ratio of the rate of fault tip propagation to the slip rate, and (6) t_{final}, the total time elapsed during deformation (Figure 5a). The number of free parameters is reduced in the model implemented here by combining v_o and t_{final} into a single parameter S, or total slip, where $v_o * t_{final} = S$ for a constant v_o and variable t_{final}. The deformation resulting from slip along a reverse fault is simulated by tracking particle paths for initially horizontal marker horizons by numeric integration of the velocity field prescribed by equation (1) as it moves along a path dictated by α and P/S, from time $t = 0$ to $t = t_{final}$.

[22] The model used in this study was validated against the forward trishear modeling program, Fault Fold© (R. D. Allmendinger, 1997–2007), which is based on the velocity field solutions presented in section 4.1. The MATLAB code replicates the resultant deformation produced using Fault Fold for the same set of input parameters with minimal misfit. Model fit to observed fold geometry is assessed by a root mean square criterion between model and observed bed dips within a cover sedimentary sequence. This approach is similar to that of *Cardozo* [2005] but does not use individual stratal thicknesses and bed position as criterion due to poor constraints on stratal thicknesses in the undeformed section in the study area. The code used in this study has the added ability to run batch forward models with no limitations on the number or location of model beds and observed dip data.

4.3. Model Setup and Selection of Parameter Space

[23] Forward models were run to simulate the deformation of initially planar, gently seaward dipping strata overlying rigid basement containing a planar fault. The total stratigraphic thickness of the cover sequence was constrained from measured sections [*Suto et al.*, 2005], and where available, from core data [*Kubo et al.*, 2002]. The total thickness of the Cretaceous through Pliocene sedimentary section at section A-A′ at the southern tip of the Futaba fault (Figure 3a) ranges from 2200 to 3000 m. A most likely thickness of 2800 m is used in the model of section A-A′. The thickness of the sedimentary section at section B-B′ across the footwall syncline (Figure 3b) is poorly constrained, and could range from 800 to 2200 m [*Kubo et al.*, 2002]. A mean sedimentary thickness of 1500 m is used in the model of section B-B′.

Table 1. Input Kinematic Model Parameter Distributions for Monte Carlo Simulations of Fold Geometry Along Sections A-A′ and B-B′

Trishear Parameter	Section A-A′		Section B-B′
	First Round	Second Round	
Total slip (S) (m)	1200–1400	1600–3600	50–2000
Ramp angle (α)	30°–89°	50° ± 12°	45 ± 8°
Trishear angle (ϕ)	40°–130°	100° ± 15°	40°–130°
Propagation to slip ratio (P/S)	0.5–3.0	0.6 to 2.2	0.5–2.5
Initial fault tip position (y)[a] (m)	−4400 to −2700	−4000 to −2700	−2500 to −0
Final fault tip position (x)[b] (m)	−2000 to 200	−1000 to 200	−8800 to −9500

[a]Position is meters below sea level.
[b]Position is 0 m at coastline.

[24] The two trishear parameters necessary to calculate rates of fault slip, throw, and shortening are fault ramp angle (α) and total slip (S). To determine the best values for S and α, Monte Carlo simulations were run for a range of α, ϕ, P/S, tip_x, tip_y, and t_{final} to determine parameter values that produce a fold geometry consistent with observed bedding positions along a surface transect. Input values for Monte Carlo simulations of hanging wall anticline at the southern tip of the Futaba fault at section A-A′ were randomly selected from uniform prior distributions (Table 1). Minimum and maximum bounds for ramp angle (30°W–89°W) were chosen to span the ramp angles of 35° to 70° and 80° to 90° proposed in previous tectonic studies of the regions surrounding the Abukuma massif [*Mitsui*, 1971; *Fukushimaken*, 1999] and the steep ramp angle suggested by field observations. Minimum and maximum bounds for ϕ (40°–130°) and P/S (0.5–3.0) were selected based on preliminary results from prior model runs.

[25] The position of the initial fault tip was calculated from fault ramp angle and present-day fault tip position. The range of depths for initial fault tip position, tip_y, was selected to be no shallower than the base of the Neogene cover sequence, and minimum and maximum bounds (−4400 to −2700 m below sea level) were constrained by results from prior model runs. The position of the present-day fault tip along section A-A′ can be constrained by projecting the tip line defined by the southernmost known outcrop of the Futaba fault south along strike into the plane of the modeled section. Uncertainties on fault tip position in the section define bounds for the present-day x coordinate of the fault tip to within 2 km of the coastline. A present-day x coordinate of the fault tip was randomly selected from this range and used in combination with fault ramp angle and initial depth of fault tip (tip_y) for each Monte Carlo simulation to calculate the x coordinate of the initial fault tip (tip_x).

[26] Forward models of the hanging wall anticline at section A-A′ were run for 40,000 combinations of input parameters for multiple values of total slip ranging from 1200 to 4000 km in 50 m increments, resulting in a total of ~1.5 million simulations. The range of total slip was selected to bracket the range of slip required to exhume the basement-cover contact, given constraints on the initial fault tip position and thickness of the sedimentary section. Best fit model parameters from this set of models were used to further constrain the distributions of input parameters for a second set of Monte Carlo simulations. Forward models were run for 25,000 additional combinations of input parameters selected from uniform distributions for total slip, propagation to slip ratio, and fault tip position, and Gaussian distributions for ramp angle and trishear angle based on the mean and standard deviation of best fit results from the initial set of models (Table 1). Models were run for multiple values of total slip ranging from 1600 to 3600 km in 50 m increments, resulting in a total of ~2.5 million fold simulations.

[27] A second section across the footwall syncline at section B-B′ was similarly modeled using the same uniform parameter bounds for ϕ (40°–130°) and P/S (0.5–2.5) as for section A-A′ and a depth range of the initial fault tip, tip_y of 2500–0 m below sea level (Table 1). Ramp angles for model of the footwall syncline along section B-B′ were randomly chosen from the Gaussian distributions of most likely ramp values obtained from modeling of the hanging wall anticline. Forward models of the footwall syncline were run for 20,000 combinations of unique parameters for total slip ranging from 50 m to 2 km in 50 m increments, resulting in ~1 million model runs.

4.4. Determination of a Best Fit Model

[28] Best fit ranges for fault ramp angle and total slip were determined from trishear model parameter sets that produce a subsurface fold and fault geometry that minimizes the misfit between observed bed dips and output model slopes along a surface profile (Figure 5b). The assessment of model fit was restricted to bedding data from the pregrowth section along a topographic profile, due of a lack of independent geophysical or borehole data that could constrain subsurface bed geometry. Structural data were collected from two sections across the hanging wall anticline at the southern tip of the Futaba fault, and from two sections across the footwall syncline ~40 km north of the southern fault tip. A combination of new field bedding data and existing map data along section A-A′ (Figure 3a) were used to constrain forward models of the hanging wall anticline. New field bedding data from the northern transect along section B-B′ were used to constrain forward models of the footwall syncline (Figure 3b).

[29] A root mean square (RMS) fit was calculated for each unique combination of tip_x, tip_y, P/S, ϕ, t_{final}, and α based on the residuals between observed bed dips and output model bed slopes. Resultant model RMS values, therefore, reflect the average deviation between observed and modeled bed dips. Given that observation error on bed dips is approximately ±5°, a set of model parameters that produced a RMS fit <5° was considered an acceptable fit that could reproduce

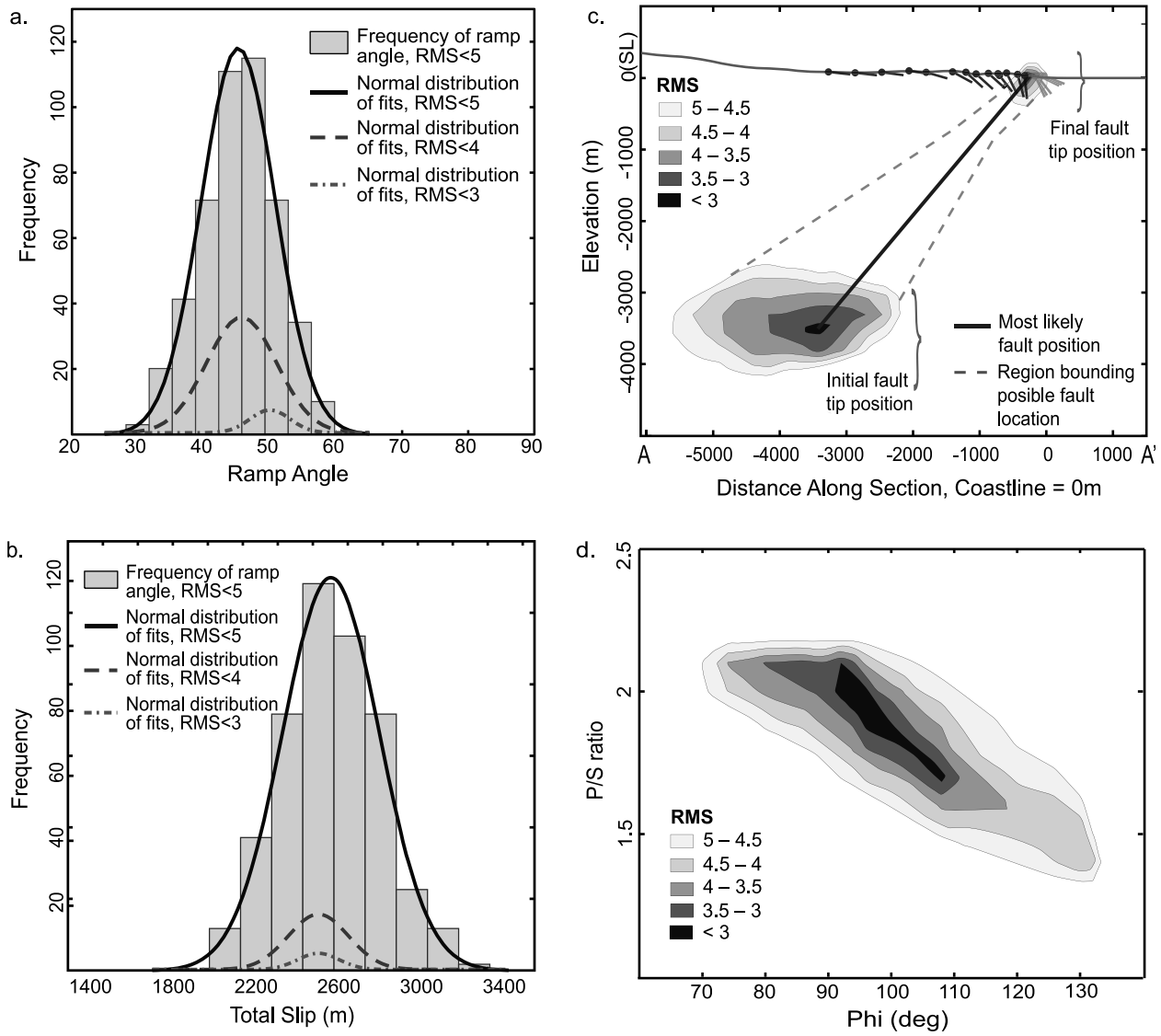

Figure 6. Most likely distributions of kinematic model parameters for fold simulations with RMS < 5° for section A-A′ across the hanging wall anticline at the southern tip of the Futaba fault. Best fit ranges of (a) fault ramp angle and (b) total slip with superimposed Gaussian distributions calculated from the mean and standard deviation for models with RMS < 5°, 4°, and 3°. (c) Most likely initial and final fault tip positions, contoured to the minimum RMS value for a given fault tip coordinate. (d) Range of most likely propagation to slip ratios (P/S) and trishear angles (ϕ), contoured to the minimum RMS value for a given parameter pair.

the observed data within error. As an additional constraint in section A-A′, models where the position of the unconformity was >20 m from its observed position were rejected. Best fit parameter ranges were determined for a section across the hanging wall anticline from models with RMS < 5° to constrain total slip and fault ramp angle at the southern tip of the Futaba fault segment.

5. Results: Shortening Along the Futaba Fault

5.1. Hanging Wall Anticline

[30] Monte Carlo simulations of forward trishear kinematic models of a section across the hanging wall anticline constrain the most likely ramp angle and total slip for the Futaba fault and define a range of optimal trishear angles, P/S ratios, and fault tip positions that simulate the observed fold. The frequency of the occurrence of values for ramp angle, trishear angle (ϕ), P/S ratio, and initial fault tip position approach Gaussian distributions centered on parameter values that simulate the most likely fault-related fold.

[31] Model simulations of the hanging wall anticline at section A-A′ that replicate observed bedding with an RMS of <5° have ramp angles that range from 31° and 60° with a most likely angle of 45 ± 6° (Figures 6a and 7 and Table 2). While a range of ramp angles can reproduce the observed dip data, simulated folds produced from gentle ramp angles of <40° underestimate the position of the basement-cover contact, and ramp angles >70° cannot reproduce beds

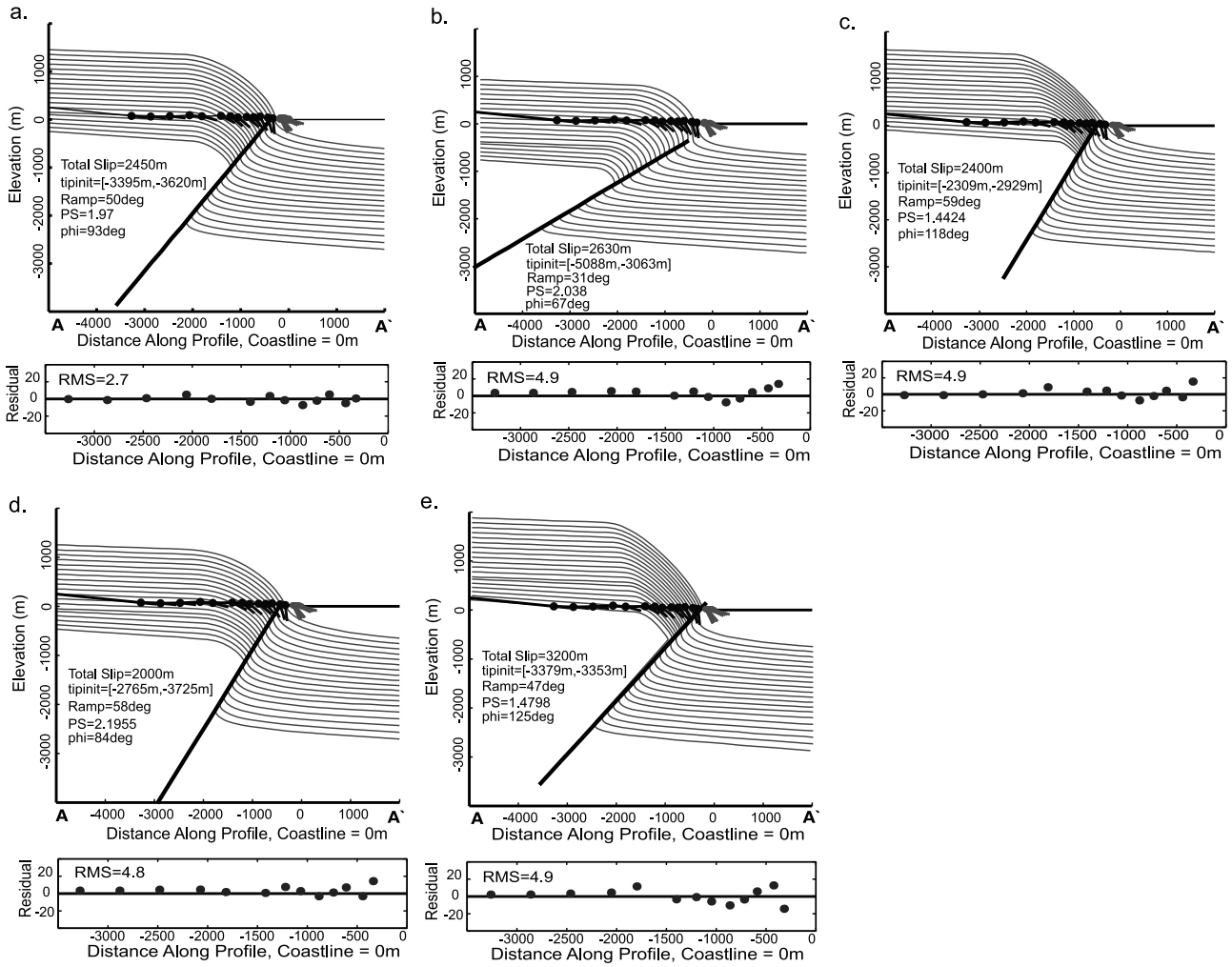

Figure 7. (a) Best fit trishear model for the hanging wall anticline along section A-A′. (top) Bedding dips in the exposed Cretaceous to Miocene predeformational strata (black dip tabs) and the position of the unconformity at the base of the Pliocene section (gray dip tabs) are used to constrain the most likely fault ramp angle and total slip for the Futaba fault. (bottom) Residuals between model bed dips and observed bed dips used to calculate RMS misfit. (b–e) Output trishear models that replicate observed bedding dips with an RMS < 5 that have the minimum and maximum allowable fault ramp angle and total slip.

overturned by 20–30°. Total dip slip required to produce model folds that replicate observed bedding ranges from 2000 to 3100 m with a mean of 2550 ± 250 m (Figures 6b and 7 and Table 2).

[32] Best fit models of the hanging wall anticline have initial fault tip positions that range in depth from 2700 to 4200 m below the surface (Figure 6c). Initial tip position is interpreted to reflect the position of the fault tip at the point at which trishear-like deformation commences, and best fit results bracket the inferred depth to the basement-cover contact of ~3000 m. Optimal initial fault tip depth varies with fault ramp angle such that models simulated for steeper ramp angles require a shallower initial fault tip.

[33] The Futaba fault is blind beneath the hanging wall anticline at the southern tip of the Namie segment, but best fit fault related fold models predict a relatively narrow range of present-day (final) fault tip positions within a ~750 m wide horizontal window no more than 500 m below the

Table 2. Mean and Standard Deviation for Best Fit Trishear Model Parameters Obtained From Monte Carlo Simulations of the Hanging Wall Anticline at Section A-A′ and of the Footwall Syncline at Section B-B′

Trishear Parameter	A-A′[a]	B-B′[b]
Total slip (S) (m)	2550 ± 250	500–1500
Ramp angle (α)	45° ± 6°	46° ± 8°
Trishear angle (ϕ)	96° ± 13°	80° ± 15°
Propagation to slip ratio (P/S)	1.9 ± 0.2	0.5–2.5
Initial fault tip position (x)[c] (m)	−3650 ± 600	−2500 to −150
Initial fault tip position (y)[d] (m)	−3300 ± 250	−12550 to −9250
Final fault tip position (x)[c] (m)	−250 ± 100	—
Final fault tip position (y)[d] (m)	−25 ± 100	—

[a]Results for 747 models with RMS < 5.
[b]Results for 1153 models with RMS < 10. Minimum and maximum values reported for non-Gaussian output distributions.
[c]Position is 0 m at coastline.
[d]Position is meters below sea level.

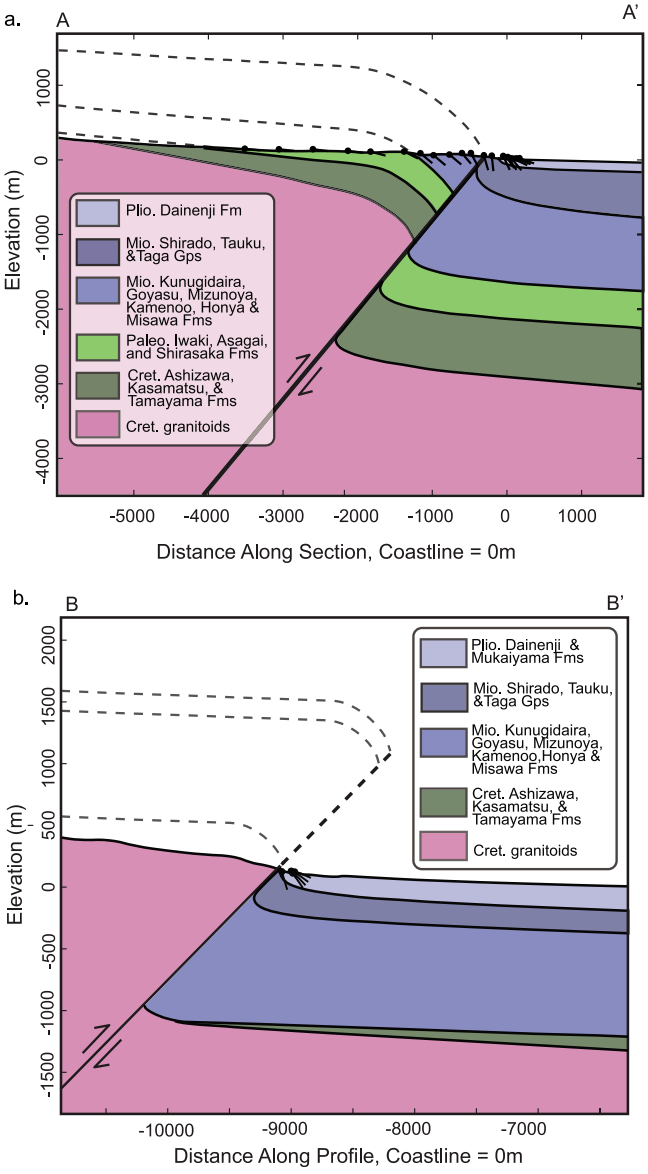

Figure 8. Cross sections across (a) the hanging wall anticline along section A-A′ and (b) the footwall syncline along section B-B′, based on results of trishear modeling. See Figures 2 and 3 for locations.

surface (Figure 6c and Table 2). The model predicted fault tip position is consistent with the projected position of the fault tip in map view from the southernmost known outcrop of the Futaba fault.

[34] Limb dips and interlimb angles of simulated folds are governed by the trishear angle (ϕ) and the *P*/*S* ratio, for a given ramp angle and total slip. Best fit models of the hanging wall anticline have trishear angles of 72°–132°, with a mean of 96° ± 13°, and *P*/*S* ratios of 1.3–2.2, with a mean of 1.9 ± 0.2 (Figure 6d and Table 2). The two parameters directly correlate such that the same model fold geometry can be simulated for a range of combinations of ϕ and *P*/*S*: large values for both ϕ and *P*/*S* can produce the same simulated fold geometry as a small values for ϕ and *P*/*S*. Best fit model fold geometries for the hanging wall anticline are used to construct a cross section across the southern Futaba fault (Figure 8a).

5.2. Footwall Syncline

[35] Modeling of the footwall syncline along section B-B′ (Figure 3b) is consistent with most likely fault ramp angle and ranges of total dip slip determined from modeling of the hanging wall anticline along section A-A′. Models of the footwall syncline were inspected for simulations with an RMS of <10° because of uncertainties in sedimentary thickness and the narrow width of the zone of deformation that limit the ability to model fold geometry to within an RMS of <5°. The most likely fault ramp angle for the footwall syncline section is 46 ± 8°, consistent with the 45 ± 6° ramp angle obtained from models of the hanging wall anticline (Table 2). Model simulations of the footwall syncline predict at least 500–1500 m dip displacement (Table 2). However, because slip can occur without further limb rotation in the trishear model once the fault tip propagates beyond the measured section, model-constrained slip is a minimum estimate. Dip displacement is better constrained by the position of nearly vertical beds in the Goyasu Formation near the base of the Yunagaya Group within the steep limb of the fold north of section B-B′ (Figure 3b), which requires a minimum stratigraphic separation across the fault of 1500–1700 m.

[36] Best fit models predict an initial fault tip position <700 m below the surface, much shallower than the range obtained from models of the hanging wall anticline and from stratigraphic separation of the Goyasu Formation. This suggests that the fault may have propagated rapidly to near the top of the cover sequence prior to the deposition of the Pliocene units deformed within the footwall syncline. The footwall syncline is best fit fit by slightly tighter trishear angles (80 ± 15°) than the hanging wall anticline (Table 2), which implies that the fold would also be fit by high *P*/*S* rations. Best fit model fold geometries are used to construct a cross section of the footwall syncline at section B-B′ (Figure 8b).

5.3. Deformation Rates

[37] The time of onset of slip along the Futaba fault is bracketed by stratigraphic horizons of known age, determined from existing tephrachronology and biostratigraphy, in units above and below the unconformity at the southern tip of the Futaba fault. A minimum age of fault initiation is obtained from the age of tephra horizon SF4.5 near the base of the postunconformity section, Dainenji Formation, upper Sendai Group. Petrographic characteristics, chemical composition, and a detailed Pliocene microfossil biostratigraphy have been used to correlate SF4.5 to the 3.95 ± 0.2 Ma An85 bed of Znp-Ohta ash [*Nagahashi et al.*, 2004]. A maximum age of fault initiation is obtained from a tephra horizon near the top of the predeformational section in the lower Sendai Group, which is chemically correlated to a tephra with a zircon fission track age of 5.6 ± 0.5 Ma in the Kameoka Formation [*Yoshida*, 1998].

[38] Best fit values for dip slip of 2.55 ± 0.25 km and fault ramp angle of 45 ± 6° combined with a time of onset of deformation of 5.6 ± 0.5 and 3.95 ± 0.2 Ma provide con-

Table 3. Average Deformation Rates for the Futaba Fault

	Initiation of Fault Slip (Ma)	Dip Slip Rate (mm/yr)	Uplift Rate (mm/yr)	Shortening Rate (mm/yr)
Maximum age	5.6 ± 0.5[a]	0.46 ± 0.06	0.32 ± 0.05	0.32 ± 0.04
Minimum age	3.95 ± 0.2[b]	0.65 ± 0.07	0.46 ± 0.07	0.46 ± 0.05
Published values	—	0.05–0.15[c]	0.5–0.6[d]	—

[a]*Yoshida* [1998] and *Suto et al.* [2005].
[b]*Nagahashi et al.* [2004].
[c]*Fukushimaken* [1999].
[d]*Suzuki* [1989].

straints on average displacement rates during the Pliocene. The best fit geometry and total dip slip predict total vertical displacement of 1800 ± 240 m and total shortening of 1800 ± 160 m. Combining these values with a minimum and maximum age of initiation of fault slip yields slip rates between 0.46 ± 0.06 to 0.65 ± 0.07 mm/yr, throw rates of 0.32 ± 0.05 to 0.46 ± 0.07 mm/yr, and shortening rates of 0.32 ± 0.04 to 0.46 ± 0.05 mm/yr (Table 3).

6. Discussion

6.1. Geometry and Kinematics of the Futaba Fault

[39] New structural field data and forward kinematic modeling of the fault related fold associated with the Futaba fault are consistent with ~2.5 km of Plio-Quaternary dip slip along a steep (40°–55°), basement-involved fault. This amount of dip slip is much greater than the vertical component of deformation previously recognized for the Futaba fault [e.g., *Mitsui*, 1971; *AIST*, 2008] and requires a nonvertical fault geometry. Kinematic models with steep ramp angles can reproduce the observed fold geometry along transects across the hanging wall anticline at the southern tip of the Namie segment of the Futaba fault and the footwall syncline along the central portion of the Namie segment. In addition, simulated fault ramp angles between 40°–55° W are consistent with fault orientation inferred in the field from shear planes and minor faults observed within hanging wall rocks. Folds simulated for ramp angles greater than ~70° W cannot produce the degree of overturning (20°–30°) observed at locations within the forelimb of the fold, such as north of transect B-B′ (Figures 3b). These results suggest that the subsurface fault ramp angle for the Futaba fault is likely 20–30° gentler than published values for the surface dip of the fault estimated from trenching.

[40] This fault geometry and displacement indicate that the Futaba fault accommodated significant contractional deformation during the late Neogene, in addition to previously recognized Quaternary strike slip. Fold reconstructions require 2.0 to 3.1 km of dip slip to generate the anticline at the southern tip of the Futaba fault, and stratigraphic separation along the northern transect is consistent with a minimum of 1.8 to 2.6 km of dip slip along a fault with a 40–55° westward dip. Extrapolation of the published left-lateral strike-slip rate of 0.15 m/ka since a 3.95–5.6 Ma onset of deformation generates only 0.6 to 0.8 km of strike displacement. These data suggest that the Futaba fault is largely characterized by Neogene reverse or oblique reverse slip.

[41] The magnitude of dip slip required to generate the fault-related fold is greater than the maximum 200 m of displacement cited in initial characterization of the fault [*Mitsui*, 1971] and the <50 m of stratigraphic separation along minor faults along the southern portion of the Futaba fault [*Kubo et al.*, 2003]. This discrepancy likely reflects that deformation at the southern tip of the Futaba fault is accommodated by folding of the cover sequence and stratigraphic thinning in the forelimb until the fault tip propagates through the fold. For faults with slow fault propagation rates in the trishear kinematic model, bed offset decreases toward the fault tip, and stratigraphic separation near the fault tip reflects only a portion of total fault slip.

[42] The transition in fault-related fold geometry from the south, where a broad anticline is developed in the hanging wall of a blind thrust (Figures 3a and 4b), to the north, where a narrow syncline is developed in the footwall of an emergent thrust (Figures 3b and 4c), is interpreted to reflect along-strike differences in fault propagation rates related to a northward thinning of the sedimentary cover sequence. The cover sequence at the southern tip of the Futaba fault is upward of 2.5 km thick, and slip along the fault is accommodated largely by folding of the cover sequence rather than by slip along a discrete fault. To the north however, the sedimentary cover sequence decreases to an average of 1.5 km thick, and is locally as thin as 800 m [*Kubo et al.*, 2002]. At this location, the fault tip likely propagates rapidly toward the surface and cuts off the steep forelimb of the fold, resulting in little folding in the hanging wall.

[43] Average dip slip rates of 0.46–0.65 mm/yr determined from kinematic modeling of the Namie segment of the Futaba fault are 5 to 10 times greater than 0.05–0.1 mm/yr determined from offset Quaternary deposits at a trench across the Haramachi segment, located ~70 km north of section A-A′ (Table 3) [*Fukushimaken*, 1998, 1999]. Rock uplift rates determined from marine terraces near the southern tip of the Futaba fault, however, agree well with model-derived results (Table 3). Stage 5e marine terrace treads preserved in the hanging wall of the Futaba fault south of section A-A′ are at elevations of ~60 m above sea level [*Kioke and Machida*, 2001]. Extrapolation of nearby strandlines predicts minimum elevations for stage 5e strandlines of 60–70 m above sea level in the Futaba hanging wall and minimum Quaternary rock uplift rates of 0.5–0.6 mm/yr [*Suzuki*, 1989]. These uplift rates are comparable to the 0.3–0.4 mm/yr throw rates determined from best fit models (Table 3) and suggest that Holocene slip rates derived from trench records may underestimate geologic average slip rates.

[44] The discrepancy in slip rate inferred from our results and that derived from paleoseismic studies may reflect the following:

[45] 1. A difference between displacement on the most recent event and the long-term slip history. This would imply that Holocene slip is not characteristic of Plio-Quaternary average slip on the Futaba fault, and would argue for the potential for temporally variable recurrence intervals and clustered events.

[46] 2. Along-strike variation in fault kinematics, which would imply a decrease in the magnitude of dip slip and an

increase in the obliquity of slip from the southern tip of the Namie segment north toward the Haramachi segment. This could be related to slip transfer across the step over from the Haramachi to the Watari segment.

[47] 3. The result of modeling a potentially complex fault zone at depth as a single fault. If deformation is the result of slip along multiple subparallel fault strands, slip rates for the single trenched segment would represent deformation along one strand, whereas the model would simulate the integrated deformation of all strands.

6.2. Implications for Plate Boundary Processes

[48] Neogene inversion of Miocene extensional structures has been argued for several thrust faults in the upper plate of northeastern Honshu, including a system of faults at the northern limit of the Futaba fault near Sendai [*Sato et al.*, 2002; *Kato et al.*, 2006]. The northward projection of the active Haramachi segment of the Futaba fault places Miocene sediments and volcanics in the hanging wall in fault contact with a ridge of granitic basement named the Wariyama uplift (Figure 1). The Miocene section to the west of the Wariyama uplift has been interpreted as a Miocene graben, and the northern Watari segment of the Futaba fault has been interpreted to link at depth with the reactivated Miocene basin-bounding fault [*Sato et al.*, 2002]. In addition, sedimentary subbasins at the southern tip of the Futaba fault have been interpreted as Miocene fault-bound basins [*Mitsui*, 1971]. The Plio-Quaternary rock uplift and exhumation of the Abukuma massif is here interpreted to be part of this system of inverted Miocene extensional half grabens, where slip along the Futaba fault is accommodated by thrust reactivation of a preexisting normal fault on the eastern flank of the massif. This interpretation is consistent with slip along a steep, west dipping fault and would predict the greatest amount of rock uplift in the hanging wall immediately adjacent to the Futaba fault.

[49] Although shortening has not previously been documented in the fore arc of northeastern Honshu, these results suggests that the Futaba fault accommodates ~0.3–0.5 mm/yr of Plio-Quaternary shortening across the fore arc. In addition, numerous mapped thrust faults north and west of the Abukuma massif are actively shortening the fore arc, and uplifted marine terraces east of the Abukuma massif [*Suzuki*, 1989] argue for the existence of at least one additional thrust fault offshore of the Abukuma massif. The Futaba fault therefore represents one fault in a system of contractional structures that actively shorten the upper plate inboard of the Japan Trench.

[50] Rates of tectonic erosion determined from reconstructions of the fore arc of erosive margins have assumed no shortening across the upper plate such that the fore-arc taper remains temporally constant. Data presented here, however, supports the accumulation of permanent strain inboard of the plate boundary and suggests that the entire fore arc acts as a deformable rather than a rigid backstop. Shortening accommodated by fore-arc structures such as the Futaba fault can cause an increase in fore-arc slope angle, flexural loading of the outer fore arc, generation of a subaqueous sedimentary basin, and an increase in offshore sedimentation rate related to onshore uplift and erosion. Therefore, the subsidence and sedimentation records used to estimate rates of tectonic erosion along the northeastern Japan margin may result from a combination of processes related to both basal erosion and upper plate shortening.

7. Conclusions

[51] New structural field data and forward trishear kinematic modeling of the fault-related folds associated with the Futaba fault collectively argue for Plio-Quaternary dip slip along a steep, basement-involved fault and may reflect contractional inversion of a Miocene extensional system. Reconstructions of fault-related fold geometry are consistent with 2.0–3.1 km of dip slip along a 40°–55° west dipping fault ramp. Tephra horizons of known age in units above and below an unconformity at the southern tip of the Futaba fault constrain the onset of deformation to between ~5.6 and ~3.95 Ma. Combining the timing of fault initiation with best estimates of fault ramp angle and total slip yields slip rates of 0.5–0.7 mm/yr, throw rates of 0.3–0.5 mm/yr and shortening rates of 0.3–0.5 mm/yr for the southern segment of the Futaba fault.

[52] The Futaba fault is one fault of a system of fore-arc contractional structures that contributes to active shortening of the upper plate inboard of the Japan Trench. The northeastern Japan margin has classically been interpreted as an erosive margin, and rates of basal erosion have been calculated assuming offshore subsidence occurs outboard of a nondeformable fore arc with constant fore-arc slope angle. However, evidence presented here supports late Neogene shortening of the upper plate and suggests that fore-arc taper may be temporally variable and that outer fore-arc subsidence along this margin occurs outboard of a deformable backstop.

[53] **Acknowledgments.** Funding for this project has been provided by the National Science Foundation Tectonic Program grant EAR-0809939, Geologic Society of America Graduate Research Grants, the P.D. Krynine Memorial fund, and the Conoco Phillips Graduate award. A special thanks to Gaku Kimura and Hiroki Watanabe for invaluable assistance and hospitality, Hiroshi Sato for valuable insights about regional tectonics, Kristin Morell for assistance in the field and lab, and Kevin Furlong for contributions to early versions of the manuscript.

References

National Institute of Advanced Industrial Science and Technology (AIST) (2008), Online active fault database of Japan, http://riodb02.ibase.aist.go.jp/activefault/index_e.html, Tsukuba, Japan.

Allmendinger, R. W. (1998), Inverse and forward numerical modeling of trishear fault-propagation folds, *Tectonics*, *17*(4), 640–656, doi:10.1029/98TC01907.

Arthur, M. A., R. von Huene, and C. G. Adelseck (1980), Sedimentary evolution of the Japan fore-arc region off northern Honshu, legs 56 and 57, *Initial Rep. of Deep Sea Drill. Proj.*, *56–57*, Part 1, 521–612.

Awata, Y. (1988), Shortening deformation of the inner zone of the northeast Japan Arc and movement of the Pacific plate (in Japanese), *Earth Mon.*, *10*, 587–591.

Cardozo, N. (2005), Trishear modeling of fold bedding data along a topographic profile, *J. Struct. Geol.*, *27*(3), 495–502, doi:10.1016/j.jsg.2004.10.004.

Cardozo, N., K. Bawa-Bhalla, A. T. Zehnder, and R. W. Allmendinger (2003), Mechanical models of fault propagation folds and comparison to the trishear kinematic model, *J. Struct. Geol.*, *25*(1), 1–18, doi:10.1016/S0191-8141(02)00013-5.

Chishitsu, C. (2003), Geoloigcal map of Japan, scale 1:1,000,000, 3rd ed., 2nd CD-ROM version, Geol. Surv. of Jpn., Tsukuba, Japan.

Clift, P. D., and P. Vannucchi (2004), Controls on tectonic accretion versus erosion in subduction zones: Implications for the origin and recycling of the continental crust, *Rev. Geophys.*, *42*, RG2001, doi:10.1029/2003RG000127.

Erslev, E. (1991), Trishear fault-propagation folding, *Geology*, *19*, 617–620, doi:10.1130/0091-7613(1991)019<0617:TFPF>2.3.CO;2.

Finn, C. (1994), Aeromagnetic evidence for a buried Early Cretaceous magmatic arc, northeast Japan, *J. Geophys. Res.*, *99*(B11), 22,165–22,185, doi:10.1029/94JB00855.

Fukushimaken (1998), Futaba fault survey, earthquake research grants FY1997 report, *Doc. 3823*, 80 pp., Fukushima.

Fukushimaken (1999), Futaba fault survey, earthquake-related basic research grants FY 1998 report, *Doc. 3826*, 109 pp., Fukushima.

Hardy, S., and E. Finch (2006), Discrete element modelling of the influence of cover strength on basement-involved fault propagation folding, *Tectonophysics*, *415*(1–4), 225–238, doi:10.1016/j.tecto.2006.01.002.

Hikima, K., and S. Oki (2008), 2008 Iwate-Miyagi Nairiku earthquake preliminary finite fault model, Earthquake Res. Inst., Univ. of Tokyo, Tokyo.

Hiroi, Y., S. Kishi, T. Nohara, K. Sato, and J. Goto (1998), Cretaceous high-temperature rapid loading and unloading in the Abukuma metamorphic terrane, Japan, *J. Metamorph. Geol.*, *16*(1), 67–81, doi:10.1111/j.1525-1314.1998.00065.x.

Ikeda, Y., M. Imaizumi, K. Hirakawa, T. Miyauchi, and H. Sato (2002), *Atlas of Active Faults in Japan*, Univ. of Tokyo Press, Tokyo, Japan.

Iwata, N., H. Tanaka, and Y. Kato (2000), Ar^{40}- Ar^{39} and K-Ar mineral ages of the Tabito composite mass in the southern Abukuma Mountains, northeast Japan, *J. Mineral. Petrol. Econ. Geol.*, *95*(1), 1–11, doi:10.2465/ganko.95.1.

Johnson, A., and R. Fletcher (1994), *Folding of Viscous Layers: Mechanical Analysis and Interpretation of Structures in Deformed Rock*, Columbia Univ. Press, New York.

Johnson, K., and A. M. Johnson (2002), Mechanical models of trishear-like folds, *J. Struct. Geol.*, *24*(2), 277–287, doi:10.1016/S0191-8141(01)00062-1.

Jolivet, L., K. Tamaki, and M. Fournier (1994), Japan Sea, opening history and mechanism: A synthesis, *J. Geophys. Res.*, *99*(B11), 22,237–22,259, doi:10.1029/93JB03463.

Kato, N., H. Sato, and N. Umino (2006), Fault reactivation and active tectonics on the fore-arc side of the back-arc rift system, NE Japan, *J. Struct. Geol.*, *28*(11), 2011–2022, doi:10.1016/j.jsg.2006.08.004.

Keller, G. (1980), Benthic foraminifers and paleobathymetry of the Japan Trench area, Leg 57, *Initial Rep. Deep Sea Drill. Proj.*, *56–57*, Part 2, 835–866.

Kioke, K., and H. Machida (2001), Atlas of Quaternary Marine Terraces in the Japanese Islands, Univ. of Tokyo Press, Tokyo.

Kubo, K., Y. Yanigisawa, S. Toshimitsu, Y. Banno, N. Kaneko, T. Yoshioka, and T. Takagi (2002), Geology of the Kawamae and Ide District, scale 1:50,000 *Quadrangle Ser. 7*(58–59), 136 pp., Geol. Surv. of Jpn., Tsukuba.

Kubo, K., Y. Yanigisawa, T. Yamamoto, M. Komazawa, T. Hiroshima, and S. Sudo (2003), Geological map of Japan, Fukushima, scale 1:200,000, Geol. Surv. of Jpn., Tsukuba.

Lallemand, S., P. Schnurle, and S. Manoussis (1992), Reconstruction of subduction zone paleogeometries and quantification of upper plate material losses caused by tectonic erosion, *J. Geophys. Res.*, *97*, 217–239, doi:10.1029/91JB02342.

Machida, H. H. (1999), The stratigraphy, chronology and distribution of distal marker-tephras in and around Japan, *Global Planet. Change*, *21*(1–3), 71–94, doi:10.1016/S0921-8181(99)00008-9.

Mitsui, S. (1971), Studies on the mechanism and deformation of sedimentary rocks in the Iwaki area of the Jaban coal-field, Fukushima Prefecture, *Sci. Rep. Tohoku Univ., Ser. 2, Geology*, *42*(3), 199–272.

Nagahashi, Y., T. Takahashi, Y. Yanagisawa, K. Kurokawa, and T. Yoshida (2004), Widespread tephra beds in the Pliocene Dainenji Formation in the Pacific coast, Fukushima Prefecture, northeastern Japan, *Earth Sci.*, *58*(5), 337–344.

Nasu, N., R. von Huene, Y. Ishiwada, M. Langseth, T. Bruns, and T. Honza (1980), Interpretation of multi channel seismic reflection data, legs 56 and 57, Japan Trench transect, *Initial Rep. Deep Sea Drill. Proj.*, *56–57*, 489–504.

Niitsuma, N. (2004), Japan Trench and tectonics of the Japanese island arcs, *Isl. Arc*, *13*, 306–317, doi:10.1111/j.1440-1738.2003.00427.x.

Ohtani, T., N. Shigematsu, K. Fujimoto, T. Tomita, and H. Iwano (2004), Geochronological constraint on the brittle-plastic deformation along the Hatagawa fault zone, NE Japan, *Earth Planets Space*, *56*(12), 1201–1207.

Sato, H. (1994), The relationship between late Cenozoic tectonic events and stress field and basin development in northeast Japan, *J. Geophys. Res.*, *99*(B11), 22,261–22,274, doi:10.1029/94JB00854.

Sato, H., and K. Amano (1991), Relationship between tectonics, volcanism, sedimentation and basin development, late Cenozoic, central part of northern Honshu, Japan, *Sediment. Geol.*, *74*(1–4), 323–343, doi:10.1016/0037-0738(91)90071-K.

Sato, H., T. Imaizumi, T. Yoshida, H. Ito, and A. Hasegawa (2002), Tectonic evolution and deep to shallow geometry of Nagamachi-Rifu active fault system, NE Japan, *Earth Planets Space*, *54*(11), 1039–1043.

Scholl, D. W., R. von Huene, T. L. Vallier, and D. G. Howell (1980), Sedimentary masses and concepts about tectonic processes at underthrust ocean margins, *Geology*, *8*(12), 564, doi:10.1130/0091-7613(1980)8<564:SMACAT>2.0.CO;2.

Seno, T., S. Stein, and A. Gripp (1993), A model for the motion of the Philippine Sea plate consistent with NUVEL-1 and geological data, *J. Geophys. Res.*, *98*(B10), 17,941–17,948, doi:10.1029/93JB00782.

Suto, I., Y. Yanagisawa, and K. Ogasawara (2005), Tertiary geology and chronostratigraphy of the Joban area and its environs, northeastern Japan, *Geol. Surv. Res. Rep. 56*(11–12), pp. 375–409, Natl. Inst. of Adv. Ind. Sci. and Technol., Tsukuba, Japan.

Suzuki, T. (1989), Late Quaternary crustal movements deduced from marine terraces and active faults, Japan coastal region, northeast Japan, *Geogr. Rep.*, *24*, pp. 31–42, Tokyo Metrop. Univ., Tokyo.

Tomita, T. T., T. Ohtani, N. Shigematsu, H. Tanaka, K. Fujimoto, Y. Kobayashi, Y. Miyashita, and K. Omura (2002), Development of the Hatagawa fault zone clarified by geological and geochronological studies, *Earth Planets Space*, *54*(11), 1095.

van der Werff, W. (2000), Backarc deformation along the eastern Japan Sea margin, offshore northern Honshu, *J. Asian Earth Sci.*, *18*(1), 71–95, doi:10.1016/S1367-9120(99)00046-2.

von Huene, R., and R. C. Culotta (1989), Tectonic erosion at the front of the Japan Trench convergent margin, *Tectonophysics*, *160*(1–4), 75–90, doi:10.1016/0040-1951(89)90385-5.

von Huene, R., and S. Lallemand (1990), Tectonic erosion along the Japan and Peru convergent margins, *Geol. Soc. Am. Bull.*, *102*(6), 704–720, doi:10.1130/0016-7606(1990)102<0704:TEATJA>2.3.CO;2.

von Huene, R., and D. W. Scholl (1991), Observations at convergent margins concerning sediment subduction, subduction erosion, and the growth of the continental crust, *Rev. Geophys.*, *29*(3), 279–316, doi:10.1029/91RG00969.

von Huene, R., et al. (1978), Japan Trench transected on Leg 57, *Geotimes*, *23*(4), 16–21.

von Huene, R., D. Klaeschen, and B. Cropp (1994), Tectonic structure across the accretionary and erosional parts of the Japan Trench margin, *J. Geophys. Res.*, *99*, 22,349–22,361, doi:10.1029/94JB01198.

Wesnousky, S. G., C. H. Scholz, K. Shimazaki, and T. Matsuda (1984), Integration of geological and seismological data for the analysis of seismic hazard; a case study of Japan, *Bull. Seismol. Soc. Am.*, *74*(2), 687–708.

Yoshida, O. M. (1998), Pleistocene fission track ages in the area north of the Kitakami Lowlands, *Res. Study Rep. 14*, 55–59, Iwate Prefectural Mus., Morioka City, Japan.

Zehnder, A. T., and R. W. Allmendinger (2000), Velocity field for the trishear model, *J. Struct. Geol.*, *22*, 1009–1014, doi:10.1016/S0191-8141(00)00037-7.

D. Fisher, E. Kirby, and C. Regalla, Department of Geosciences, Pennsylvania State University, University Park, PA 16802, USA. (dmf6@psu.edu; ekirby@psu.edu; cregalla@psu.edu)